JOC The Journal of Organic Chemistry

Article

pubs.acs.org/joc

Mechanistic Study of the Asymmetric Carbonyl-Ene Reaction between Alkyl Enol Ethers and Isatin Catalyzed by the *N,N′*-Dioxide–$Mg(OTf)_2$ Complex

Junming Wang, Zhishan Su,* Na Yang, and Changwei Hu

Key Laboratory of Green Chemistry and Technology, Ministry of Education, College of Chemistry, Sichuan University, Chengdu, Sichuan 610064, P. R. China

Supporting Information

ABSTRACT: The mechanism and origin of the stereoselectivity of the asymmetric carbonyl-ene reaction between *N*-methyl-protected isatin and 2-methyloxypropene catalyzed by the *N,N′*-dioxide–$Mg(OTf)_2$ complex were investigated by DFT and ONIOM methods. The background reaction occurred via a two-stage, one-step mechanism with a high activation barrier of 30.4 kcal mol^{-1} at the B3LYP-D3(BJ)/6-311G**(SMD, CH_2Cl_2)//B3LYP/6-31G*(SMD, CH_2Cl_2) level at 303 K. Good linear correlations between the global nucleophilicity index (*N*) and the activation energy barrier ($\Delta G^{\ddagger}$) were found. The chiral *N,N′*-Mg(II) complex catalyst could enhance the electrophilicity of the isatin substrate by forming hexacoordinate Mg(II) reactive species. The substituent at the *ortho* positions of aniline combined with the aliphatic ring of the backbone in the chiral *N,N′*-dioxide ligand played an important role in the construction of a favorable "pocket-like" chiral environment (chiral pocket) around the Mg(II) center, directing the preferential orientation of the incoming substrate. An unfavorable steric arrangement in the *re*-face attack pathway translated into a more destabilizing activation strain of the ene substrate, enhancing enantiodifferentiation of two competing pathways for the desired *R* product. This work also suggested a new phosphine ligand (**N-L1**) for the formation of the Mg(II) complex catalyst for the asymmetric carbonyl-ene reaction. The chiral environment and Lewis acidity of the Mg(II) complex could be fine-tuned by introduction of P-donor units into the ligand for highly efficient asymmetric catalysis.

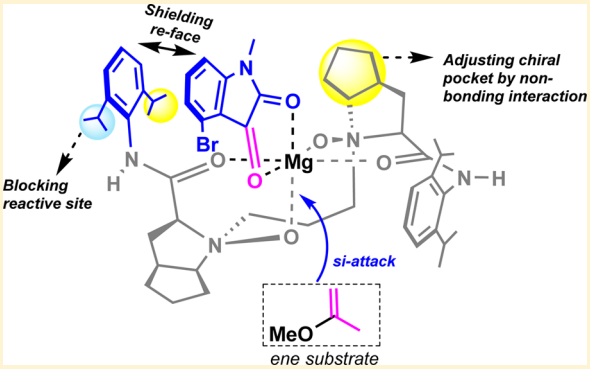

INTRODUCTION

The ene reaction provides convenient access for constructing the C–C bond, which involves the interaction between an alkene with an allylic C–H bond (an ene component) and a compound containing a multiple bond (an enophile).[1−6] The catalytic asymmetric ene reaction of carbonyl compounds has attracted much attention because it allows the atom-economic construction of a wide range of building blocks for the synthesis of functionalized products.[7] Since the pioneering work of Yamamoto and co-workers,[8] massive effort has been devoted to developing chiral Lewis acid catalysts (or promoters) for enantioselective carbonyl-ene reaction.[7] The Mikami group utilized Ti(IV)/binaphthol catalysts to realize the first catalytic asymmetric ene cyclization.[9] Later, chiral bis(oxazoline)-derived ligands combined with Cu(II),[10] Sc(III),[11] and In(III)[12] metal ions were demonstrated to be efficient in furnishing the desired products in high yields with satisfactory stereocontrol. Some late transition metal complex catalysts derived from Co,[13] Pd,[14] Pt,[14e,15] Cr,[16] and lanthanides[17] were also used successfully to mediate the asymmetric carbonyl-ene reaction under mild conditions.

The generally accepted mechanism of the ene reaction involves formation of a new σ-bond with migration of the ene double bond and allylic hydrogen.[1] For many ene reactions, the exact pathway either is not defined or proceeds by both a one-step mechanism and ionic pathway, depending on the reaction conditions.[1,18] A stepwise mechanism involving polarized diradical intermediates was preferred for highly electrophilic nitroso and triazolinedione compounds.[19] The analysis of the potential energy surface of metallo-ene reaction of allyl-metal (Li and Na) with ethylene indicated a concerted process. The metal migration path had an activation energy lower than that of hydrogen migration.[20] Intra-aryne ene reactions were computationally studied at the B3LYP/6-31G(d) level by Lautens et al., and a pseudo-chair-like transition state in a concerted process was previously proposed.[21] The electron localization function (ELF) topological analysis combined with global electron density transfer (GEDT) indicated inter- and intra-aryne ene reactions occur via a one-step mechanism by a C–C coupling of two pseudoradical centers.[22] The Lewis acid promoted carbonyl-ene reaction involved in the coordination of the carbonyl group substrate to the metal center.[1,18] A single-point binding activation model for the aldehyde substrate was

Received: May 7, 2016
Published: July 11, 2016

DOI: 10.1021/acs.joc.6b01071
J. Org. Chem. 2016, 81, 6444–6456

proposed in the presence of the dimeric tridentate Schiff base chromium(III) complex.[23] The identity and position of the substitution on the substrate might exert a significant impact on both reaction rate and enantioselectivity by defining a particularly reactive species.[23] For 1,2-dicarbonyl compounds (such as isatins), a bidentate chelating interaction with the metal center was supposed to induce high level of enantioselectivity as well as reactivity.[9c,10b,14b,17,24] The frontier molecular orbitals involved in electron transfer from ene HOMO to enophile LUMO followed by enophile LUMO transferring back to the LUMO of the C−H bond were adopted to explain the reactivity of various Lewis acids in the imine-ene reaction.[25] The activation strain arising from deformed reactants exerted an important influence on reactivity by controlling the height and trend of the energy barrier in the Alder-ene reaction.[26] In addition, the counterion effects may be another factor in the formation of more reactive species.[12a,14b,15] Domingo and co-workers discovered good correlations among activation energies, the polar character, and the global electron density transfer (GEDT) at the TSs at the MPWB1*K*/6-311g(d,p) level, and the ene reaction was classified into three types (nonpolar, polar, and ionic).[18] The steric, torsional effect and the electronic factor were supposed to effect face selectivity in the asymmetric ene reaction.[1]

Recently, Feng's group developed a novel and efficient catalyst system based on C_2-symmetric chiral *N*,*N*′-dioxide−metal complexes for asymmetric catalysis.[27] The chiral *N*,*N*′-dioxide ligand with Mg(II),[27a] Cu(II), or Ni(II)[27b] could form efficient catalysts for asymmetric heteroene reaction of 1,2-dicarbonyl compounds (including isatins, α-ketoesters, and glyoxal derivatives), using alkyl enol ethers as nucleophiles. The β-hydroxyenol ether with excellent outcomes (up to 98% yield and >99% ee) could be obtained under mild reaction conditions. Some vital structural characteristics (such as *i*Pr substituents at the *ortho* position of aniline as well as the chiral backbone) of the ligand appeared to be essential for the synthesis of target carbonyl-ene products. A transition state model from HRMS analysis was proposed to explain possible intermediate and experimental observations of stereoselective outcomes.[27a] Although these results provide valuable information for beginning the mechanistic analysis of the carbonyl-ene reaction, the character of the chiral environment around the metal ion and the origin of the asymmetric inductive effect of the chiral catalyst are still unclear. Furthermore, theoretical studies of the asymmetric carbonyl-ene reaction were very limited.[10b,17] Herein, the mechanism and stereoselectivity of the carbonyl-ene reaction between isatins and alkyl enol ethers catalyzed by the chiral *N*,*N*′-dioxide−Mg(II) complex were investigated by DFT and ONIOM methods. The effects of steric and electronic properties of the ligands on activation barriers as well as stereoselectivity were analyzed. The key structural units in the chiral ligand were explored to identify the factors controlling the enantioselectivity of the products. Furthermore, we disclose a ligand design that offers a conceptually new potentially general approach to achieving high-efficiency magnesium catalysis.

COMPUTATIONAL DETAILS

All calculations were performed by using the Gaussian 09 program package.[28] Geometries were fully optimized in the CH_2Cl_2 solvent at 303 K[27a] and characterized by frequency analysis. The self-consistent reaction field (SCRF) method based on the universal solvation model SMD was adopted to evaluate the effect of solvation on the reaction.[29] The DFT method at the B3LYP/6-31G* level was used to simulate the mechanism of background reactions. The ONIOM[30] method, combining the UFF[31] molecular mechanics force field for the low-level layer with the B3LYP[32] density functional and 6-31G(d) basis set, was used for the optimization of all stationary points in the actual catalytic system (see Scheme 1). The intrinsic reaction coordinate (IRC) path was traced to check the energy profiles connecting each transition state to two associated minima of the proposed mechanism.[33] Single-point energies were obtained for all optimized structures using the dispersion-corrected density functional [DFT-D3(BJ)].[34] Natural bond orbital (NBO),[35] reactivity index analysis (electrophilicity index ω and nucleophilicity index N)[18,36] of the reactants was performed to obtain further insight into the electronic properties of the system at the B3LYP-D3(BJ)/6-311G(d,p) level. Local electrophilicity ω_k and local nucleophilicity N_k indices were defined as $\omega_k = \omega P_k^+$ and $N_k = NP_k^-$, where the atom k electrophilic and nucleophilic Parr functions (P_k^+ and P_k^-) were from the Mulliken atomic spin density (ASD) analysis at the radical cation and at the radical anion of the corresponding reagent, respectively[37] (see Table S1). Furthermore, we have also calculated the summary of the electrophilicity index (ω) and nucleophilicity index (N) to obtain two reactivity indices, E_1 and E_2.[38] The corresponding expressions were $E_1 = \omega$(isatin) + N(ene) and $E_2 = \omega$(ene) + N(isatin), respectively (shown in Table S2). The results of activation strain model (ASM)[39] analysis on transition states in the carbonyl-ene reaction were shown in Table 2 and Table S3, in which activation energy $\Delta E^{\ddagger}$ of the transition state was decomposed into strain energy $\Delta E^{\ddagger}_{strain}$ and interaction energy $\Delta E^{\ddagger}_{int}$ (i.e., $\Delta E^{\ddagger} = \Delta E^{\ddagger}_{strain} + \Delta E^{\ddagger}_{int}$). Unless specified, the Gibbs free energies corrected by both solvation and zero-point vibrational effects at the B3LYP-D3(BJ)/6-311G(d,p)(SMD, CH_2Cl_2) level were used in the discussions.

Scheme 1. Asymmetric Addition of 2-Methyloxypropene (R2a) to *N*-Methyl-Protected Isatin (R1a and R1b) Catalyzed by the *N*,*N*′-Dioxide−Mg(OTf)$_2$ Complex

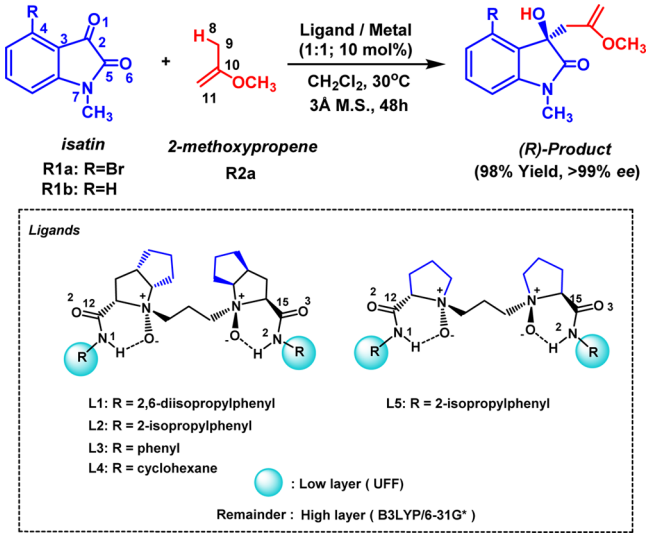

RESULTS AND DISCUSSION

Mechanism of the Background Reaction. Initially, the noncatalyzed carbonyl-ene reactions between *N*-methyl-protected isatin (**R1a** and **R1b**) and 2-methoxypropene (**R2a**) were investigated. The pathways involving the favorable *si*-face approach of **R1a** were studied as the representative case. Calculations indicated that the reaction occurred through a two-stage, one-step mechanism[40] via chairlike (or envelope) six-membered ring transition states (**B-TS$_{1a-2a}$** or **B-TS$_{1b-2a}$**), which are similar to those obtained by the groups of Houk,[41]

DOI: 10.1021/acs.joc.6b01071
J. Org. Chem. 2016, 81, 6444−6456

Bickelhaupt,[26a] and Lan[26b] in the ene reaction. The H8 atom was transferred from C9 to O1 atoms, accompanied by the formation of a C−C bond. An asynchronous mechanism with polar character was presented for these two TSs, with C11−C2 and C9−H8 distances of 1.723 and 1.227−1.229 Å, respectively. The activation energy for **R1a** via **B-TS$_{1a-2a}$** was predicted to be 30.4 kcal mol^{-1}, which was lower than that of **R1b** via **B-TS$_{1b-2a}$** by 1.2 kcal mol^{-1} (see Figure 1 and Figure S1). The isatin with an electron-withdrawing substituent Br atom (**R1a**) showed higher reactivity, which was attributed to its enhanced eletrophilicity [the electrophilicity indices (ω) were 3.03 eV for **R1a** and 2.85 eV for **R1b**]. This significant electronic effect was also observed in the experiment.[27a] The isatins with electron-withdrawing -F, -Cl, or -CF$_3$ substitutions in the proximity of the reacting C2 atom gave ω_k values (0.58−0.59 eV) similar to that of **R1a** with a Br atom (see Table S1). Compared to halogen-substituted isatin, the CF$_3$-substitued isatin exhibited a higher electrophilicity index ω (3.21 eV) and better reactivity for carbonyl-ene reactions of **R2a**, with energy barriers of 29.0 kcal mol^{-1}. Considering the fact that two carbonyl groups existed in **R1a**, another possible addition process involved in the C5═O6 bond was also studied. Calculations predicted that the energy barrier via **B-TS$_{1a-2a}$-1** was 38.3 kcal mol^{-1} (see Figure S2), which was higher than that of the pathway via **B-TS$_{1a-2a}$** (30.4 kcal mol^{-1}). This result could be explained by the fact that excess energy was needed to break the conjugation between the lone electron pair of the nitrogen atom and the adjacent C═O moiety via **B-TS$_{1a-2a}$-1**. Furthermore, electronic property analysis also indicated local electrophilicity index ω_k (0.27 eV) for nucleophilic attack at electrophilic site C5 was lower than at C2 (0.55 eV) in **R1a**, suggesting that it was an unfavorable reactive site for the addition reaction.

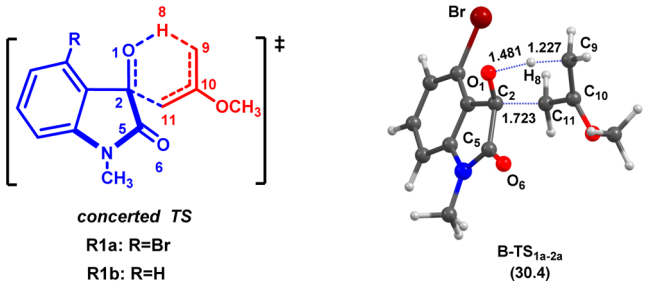

Figure 1. Optimized geometries of transition states **B-TS$_{1a-2a}$** in the carbonyl-ene reaction of **R1a** with **R2a** in the absence of catalyst. The relative Gibbs free energies are shown in parentheses (kilocalories per mole).

The carbonyl-ene reaction between **R1a** and **R2a** was characterized by electrophilicity−nucleophilicity interaction. To understand the effect of different substituents on the carbonyl-ene process, six more representative nucleophiles (**R2b−R2g**) were further studied without a catalyst. Their global indices and the corresponding local reactivity indices are listed in Table 1 and Table S1. Furthermore, we used the Eyring equation (eq 1) to predict the corresponding rate constant k in the reaction.

Table 1. Global Nucleophilicities (N, electronvolts), Electronic Chemical Potentials (μ, electronvolts), Chemical Hardnesses (η, electronvolts), and Global Electrophilicities (ω, electronvolts) of Carbonyl Compounds (R1a and R1b) and Nucleophiles (R2a−R2g) and Activation Energy Barriers ($\Delta G^{\ddagger}$, kilocalories per mole) and Reaction Rate Constants (k) for the Carbonyl-Ene Reaction of R2a−R2g toward R1a in the Absence of a Catalyst[a]

	Compounds	μ	η	ω	N	$\Delta G^{\ddagger}$	log k
R1a		-4.68	3.62	3.03	2.33	-	-
R1b		-4.54	3.61	2.85	2.47	-	-
R2a		-2.65	7.13	0.49	2.60	30.4	-9.1
R2b		-3.12	7.21	0.68	2.08	34.2	-11.9
R2c		-3.11	7.21	0.67	2.10	33.0	-11.0
R2d		-3.49	6.35	0.96	2.15	33.8	-11.6
R2e		-2.63	6.97	0.50	2.70	28.8	-8.0
R2f		-2.21	6.25	0.39	3.48	18.6	-0.6
R2g		-3.57	6.91	0.92	1.78	36.1	-13.2

[a]Calculations were conducted at the B3LYP-D3(BJ)/6-311G**(SMD, CH_2Cl_2)//B3LYP/6-31G*(SMD, CH_2Cl_2) level at 303 K.

DOI: 10.1021/acs.joc.6b01071
J. Org. Chem. 2016, 81, 6444−6456

$$k = \frac{k_B T}{h} \exp\left(-\frac{\Delta G^{\ddagger}}{RT}\right) \quad (1)$$

where k_B is Boltzmann's constant, h Planck's constant, R the gas constant, and T the temperature (T = 303 K in ref 27a).

As shown in Figure 2, the activation barrier ($\Delta G^{\ddagger}$) of carbonyl-ene reactions decreased with an increase in the nucleophilic index (N) of ene compounds. Furthermore, a good linear relationship between them was found with a regression coefficient of 0.97. The difference in the two reactivity indices, E_1 and E_2, for the isatin/ene interacting pair (i.e., $\Delta E_{12} = E_1 - E_2$) was expected to be related to the polar character of the reaction as well as the electron flow process of the reaction. For the carbonyl-ene reactions of **R1a** to **R2a**–**R2f**, $E_1 > E_2$ indicated that electronic density changed from **R2a**–**R2f** (ene component) to **R1a** (isatin) via a polar process. Interestingly, ΔE_{12} exhibited a good linear correlation with activation barriers with R^2 = 0.92 (see Figure S3). As shown in Table S2, the ΔE_{12} for **R2a** with a -OCH_3 group was higher than that of **R2b** with a -CH_3 group by 0.70 eV, which was in agreement with its lower energy barrier (30.4 kcal mol^{-1} for **R2a** vs 34.2 kcal mol^{-1} for **R2b**). The reactivity of nucleophilic ene compounds was further enhanced when a strong electron-releasing group [-N(CH_3)$_2$, **R2f**] was introduced at the C10 atom of **R2a**, with a decrease in the activation barrier by 11.8 kcal mol^{-1}. The effect of the electronic properties of the substituent of the ene moiety on the efficiency of the reaction was also observed in a theoretical investigation by Zhang and co-workers.[25]

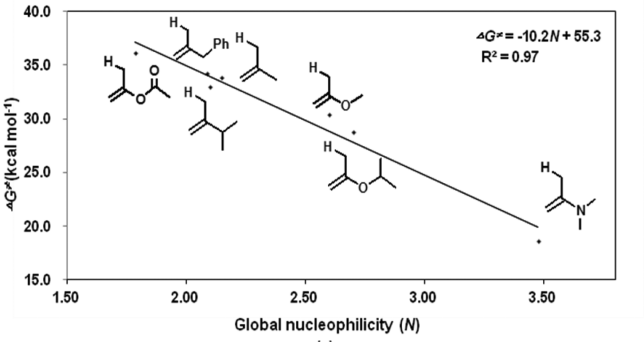

Figure 2. Correlation between the global nucleophilicity index (N) and activation energy barrier ($\Delta G^{\ddagger}$) for the carbonyl-ene reaction between **R1a** and **R2a**–**R2g** in the absence of a catalyst. $\Delta G^{\ddagger}$ = −10.2N + 55.3 (R^2 = 0.97).

The activation strain model (ASM) provided insight into the origin of reactivity variation for seven ene compounds (**R2a**–**R2g**) toward isatin **R1a**. As shown in Table 2, the differences in activation energies were mainly from strain energy ($\Delta E^{\ddagger}_{strain}$, 58.4–88.7 kcal mol^{-1}) during the formation of TSs. Furthermore, the contribution of an ene fragment to the total strain energy was larger than that of the enophile one [especially at the initial stage (Figure S4 using **R2a** as an example)], indicating more energy was required to deform the ene moiety to the TS geometries. The result was consistent with findings by Fernández and Bickelhaupt et al.[24] Interestingly, the contribution of the two fragments to strain energy became comparable, accompanied by a decrease in the activation barriers for the reactions. Meanwhile, the shift of TSs from early to late was perceptible in geometries as activation barriers dropped. When **R1a** reacted with strong nucleophilic ene compound **R2f**, the distance for the forming C–C bond was as short as 1.640 Å. The significant structural distortion (larger dihedral angle $D_{1-2-5-6}$ as well as C2═O1 band) led to increasingly destabilizing strain energy in **B-TS$_{1a-2f}$** (up to 88.7 kcal mol^{-1}). However, the more stabilizing interaction of two fragments ($\Delta E^{\ddagger}_{int}$ = −73.2 kcal mol^{-1}) compensated for the unfavorable deformation energy, accelerating the reaction with a lower activation energy (18.6 kcal mol^{-1}). Furthermore, a good linear correlation was found between the interaction energy ($\Delta E^{\ddagger}_{int}$) and the theoretical log k value with a regression coefficient of 0.93 for carbonyl-ene reactions involving seven ene compounds (see Figure S5).

Table 2. Activation Energies and Their Energy Components (kilocalories per mole) for the Addition of Ene Compounds (R2a–R2g) to R1a in the Absence of a Catalyst at TSs

			$\Delta E^{\ddagger}_{strain}$			
path	reaction	$\Delta E^{\ddagger}_{int}$	enophile (R1a)[a]	ene[b]	sum[c]	$\Delta E^{\ddagger}$[d]
1	**R1a** + **R2a** → **B-TS$_{1a-2a}$**	−47.5	33.9	39.5	73.4	25.9
2	**R1a** + **R2b** → **B-TS$_{1a-2b}$**	−29.7	25.4	33.3	58.7	29.0
3	**R1a** + **R2c** → **B-TS$_{1a-2c}$**	−30.5	25.2	33.2	58.4	27.9
4	**R1a** + **R2d** → **B-TS$_{1a-2d}$**	−31.1	24.3	35.4	59.7	28.6
5	**R1a** + **R2e** → **B-TS$_{1a-2e}$**	−51.2	35.1	40.5	75.6	24.4
6	**R1a** + **R2f** → **B-TS$_{1a-2f}$**	−73.2	43.4	45.3	88.7	15.5
7	**R1a** + **R2g** → **B-TS$_{1a-2g}$**	−32.6	27.2	35.2	62.4	29.8

[a]Strain energy of the enophile fragment (**R1a**). [b]Strain energy of the ene fragment (**R2a**–**R2g**). [c]Total strain energy. [d]Activation energy at 303 K in the gas phase.

Therefore, the reaction rate and feasibility of addition of nucleophilic ene compounds (**R2a**–**R2g**) to 1,2-dicarbonyl (**R1a** or **R1b**) were related closely to the nucleophilicity of the ene component and the electrophilicity of isatins. Furthermore, the strain energy of the ene substrate exerted an important influence on the reaction. The introduction of substituents (electron-withdrawing group to isatins or electron-donating group to enol ethers) close to the reacting sites could affect their reactivity indices and alter the reaction polar character. Even so, the energy barrier of the carbonyl-ene reaction between **R1a** and **R2a** reached up to 30.4 kcal mol^{-1}, indicating that it was difficult for the background reaction to occur in the absence of a catalyst.

Mechanism of the Catalytic Reaction. Experimental investigations achieved by X-ray analysis indicated that the *N*,*N*′-dioxide compound could behave as a neutral tetradentate ligand in which both oxygens of *N*-oxide and both carbonyl oxygens coordinate to the metal central, forming the *N*,*N*′-dioxide–Mg(II) complex.[27a] Furthermore, HRMS analysis of the dynamic intermediates in the carbonyl-ene reaction suggested that both oxygen atoms of *N*-methyl-protected isatin **R1a** interacted with central metal Mg^{2+} ion in a bidentate fashion with its dicarbonyl groups to form a hexacoordinate intermediate.[27a] On the basis of experimental observations, we started theoretical simulations of the catalytic reaction using **L1**–**COM** (as shown in Figure 3) as a staring reactive species at the B3LYP-D3(BJ)/6-311G**(SMD, CH_2Cl_2)//ONIOM-

DOI: 10.1021/acs.joc.6b01071
J. Org. Chem. 2016, 81, 6444–6456

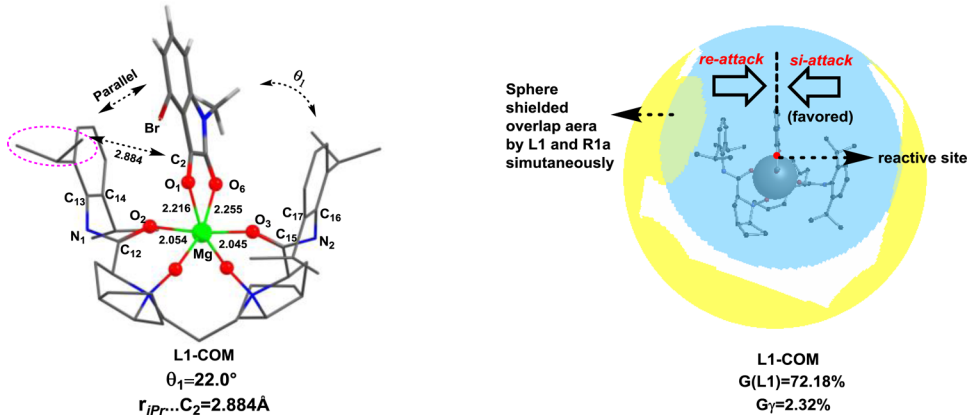

Figure 3. Optimized geometry of **L1**−**COM** and visualization of the metal center coordination sphere shielded by the *N*,*N*′-dioxide ligand **L1** (yellow area) and **R1a** (blue area) in **L1**−**COM**. G(**L1**) is the percentage of metal center coordination sphere shielded by the *N*,*N*′-dioxide ligand, obtained with the Solid-G program. G_γ is the sphere-shielded overlap area of **L1** and **R1a**, simultaneously.

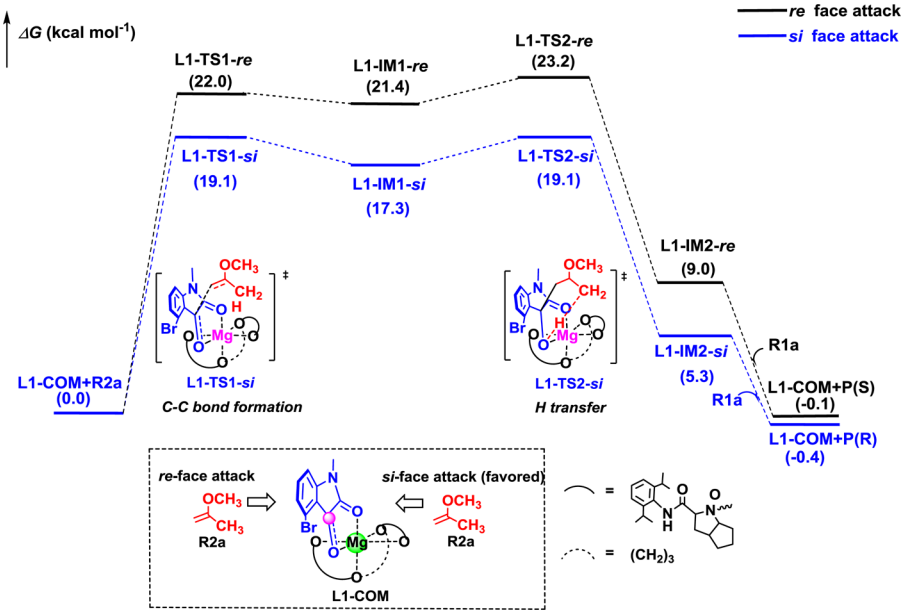

Figure 4. Energy profiles for the asymmetric carbonyl-ene reaction between *N*-methyl-protected isatin (**R1a**) and 2-methoxypropene (**R2a**) catalyzed by the **L1**−Mg(II) catalyst.

(B3LYP/6-31G*:UFF)(SMD, CH_2Cl_2) level. As expected, the formation of complex **L1**−**COM** enhanced the electrophilicity of **R1a**, with a larger global electrophilic index ω of 5.04 eV as well as a local electrophilic index ω_k of 1.38 eV on the C2 atom (3.03 and 0.55 eV, respectively, in free **R1a**). Accordingly, the ΔE_{12} of the two interacting species increased from 2.81 eV for the uncatalyzed process to 5.30 eV for the catalyzed one, indicating the enhanced polar character of the reaction and, consequently, a lower activation barrier. Different from the background reaction of **R1a**, a stepwise mechanism (not a one-step mechanism[24,42]) was adopted in the presence of the *N*,*N*′-dioxide−Mg(II) complex. C−C bond formation was achieved via two competing transition states **L1**−**TS1**-***si*** (*si*-face attack) and **L1**−**TS1**-***re*** (*re*-face attack), producing zwitterionic intermediates **L1**−**IM1**-***si*** and **L1**−**IM1**-***re***, respectively. Then, the catalytic process finished with H transfer directly from methyl group of **R2a** to the O1 atom of the **R1a** moiety, producing product−catalyst complexes (**L1**−**IM2**-***si*** and **L1**−**IM2**-***re***). The C−C bond formation step was predicted to be the chirality-controlling step for the entire reaction. Because of the breaking of the conjugated interaction in free **R1a**, the relative energies for resultant **L1**−**IM1**-***si*** and **L1**−**IM1**-***re*** were slightly lower than those for the corresponding C−C bond formation transition states. These highly polar structures in Lewis acid-catalyzed reactions have also been reported in our previous work.[43] Compared to that of the background reaction, the activation barriers of the catalytic one were significantly decreased (by 11.3 and 8.4 kcal mol^{-1}). Therefore, the chiral *N*,*N*′-dioxide−Mg(II) catalyst played an important role in favoring the reaction through a more polar process by increasing the electrophilicity of isatin through the coordination of Lewis acid to a carbonyl group of isatin. As shown in Figures 4 and 5, the energy barriers corresponding to the attack of nucleophile **R2a** from the *si*-face were lower in two steps, giving predominantly the *R*-configured product. According to the Curtin−Hammett principle,[44] the predicted selectivity (ee %) was 99.9% (Table S4), which agreed well the experimental observation (>99% ee).[27a] We also evaluated two more theoretical levels, reoptimized all transition states, and performed single-point calculation using DFT methods at the

DOI: 10.1021/acs.joc.6b01071
J. Org. Chem. 2016, 81, 6444−6456

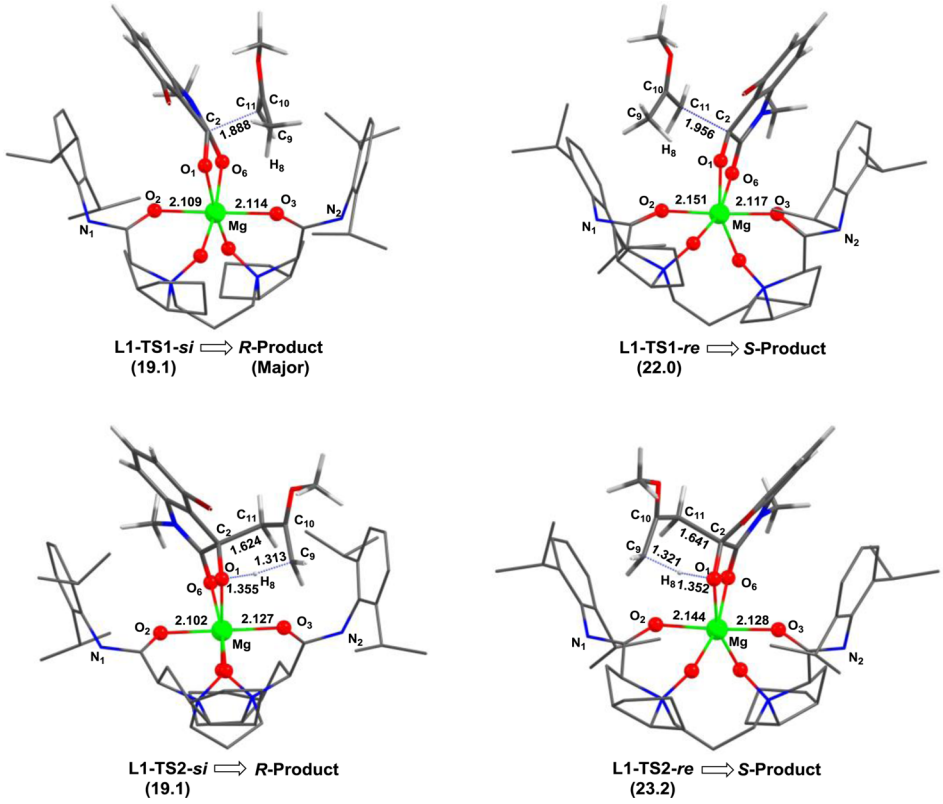

Figure 5. Optimized geometries of transition states and their relative Gibbs free energies (kilocalories per mole) in the carbonyl-ene reaction between *N*-methyl-protected isatin (**R1a**) and 2-methoxypropene (**R2a**), catalyzed by the **L1**−Mg(II) complex catalyst.

B3LYP-D3(BJ)/6-311G**(SMD, CH_2Cl_2)//B3LPY-D3(BJ)/6-31G**(SMD, CH_2Cl_2) and M06-2X/6-311G**(SMD, CH_2Cl_2)//M06-2X/6-31G**(SMD, CH_2Cl_2) levels, respectively. Similar results (mechanism and geometries of TSs) were obtained (see Table S5 and coordinates in the Supporting Information), although larger energy differences of two competing TSs in the chirality-controlling step were obtained. Considering the computational cost, the present theoretical level was used for the following calculations. Note that the activation energy barriers for two H transfer steps were the same (1.8 kcal mol^{-1}), which were lower than those of the first chirality-controlling steps (19.1 and 22.0 kcal mol^{-1}). The relative energy of **L1**−**IM1-*re*** was higher than that of **L1**−**IM1-*si*** because of steric hindrance between the methyl group of **R2a** and the isopropyl substituent of **L1**. Compared to that in **L1**−**IM1-*re*** (1.320 Å), the O1−C2 bond in **L1**−-**IM1-*si*** was weakened significantly (1.335 Å), leading to a lower relative energy of **L1**−**TS2-*re*** in the following H transfer step.

Stereocontrol of the Chiral Catalyst. Structural analysis helped us to understand the stereoselectivity of the asymmetric carbonyl-ene reaction catalyzed by the *N*,*N*′-dioxide−Mg(II) complex. As shown in Figure 3, coordination of the ligand to the Mg(II) center forms a "pocketlike" chiral environment (chiral pocket), in which two amide subunits lie out of the horizontal O2−Mg−O3 plane, front right and rear left.[27c,d] The isopropylphenyl group on the left brachial amide of the ligand paralleled the planar **R1a** substrate, almost shielding the *re*-face of it. Most importantly, the neighboring bulky isopropyl (*i*Pr) group blocked the reactive site C2 atom in the **R1a** substrate, with a distance of 2.884 Å (shown in Figure 3). With the compound suffering from steric blocking from the isopropylphenyl group (especially the bulky *i*Pr group on the left amide), the *re*-face attack of **R1a** became unfavorable. A more significantly structural deformation was observed in the formation of **L1**−**TS1-*re***, in which the amide group of ligand moved away from Mg^{2+} center, leading to an O2−Mg bond 0.097 Å longer than that of **L1**−**COM**. However, a less sterically crowded arrangement was found for the *si*-face of **R1a**. The angle between planar **R1a** and the right isopropylphenyl group (θ_1) was 22.0°, providing more opening space for attack of another substrate, **R2a**. For **L1**−**TS1-*si***, the methyl group of **R2a** was placed in the middle of the diisopropylphenyl group in the amide moiety of the ligand (**L1**), preventing steric repulsion from two neighboring isopropyl groups. Thus, **R1a** could interact well with **R2a**, with larger interaction energies [−33.2 kcal mol^{-1} (Table S3)]. Accordingly, the relative energy of **L1**−**TS1-*si*** was 2.9 kcal mol^{-1} lower than that of **L1**−**TS1-*re***.

A complete diagram of activation strain analysis along reaction coordination (C11−C2 bond formation process) allowed us to rationalize deeply the preferred *si*-face attack over *re*-face attack pathway in the asymmetric carbonyl-ene reaction mediated by the **L1**−Mg(II) complex. As shown in Figure 6a, the interaction ΔE_{int} values between fragments were comparable for *si*-face attack and *re*-attack pathways in the reaction process. The main difference in the activation barrier for the two competing pathways arose from the strain energy term, ΔE_{strain}. Moreover, the strain energy corresponding to the *si*-face attack pathway was less destabilizing at any given point along the reaction coordinate than the *re*-face attack one, which was responsible for the lower reaction barrier of the favorable *si*-face attack pathway. The total ΔE_{strain} was further decomposed into three energy contributors, including deformation energies of the catalyst (Cat), **R1a** and **R2a** (shown in Figure 6b). With respect to favorable *si*-face attack,

DOI: 10.1021/acs.joc.6b01071
J. Org. Chem. 2016, 81, 6444−6456

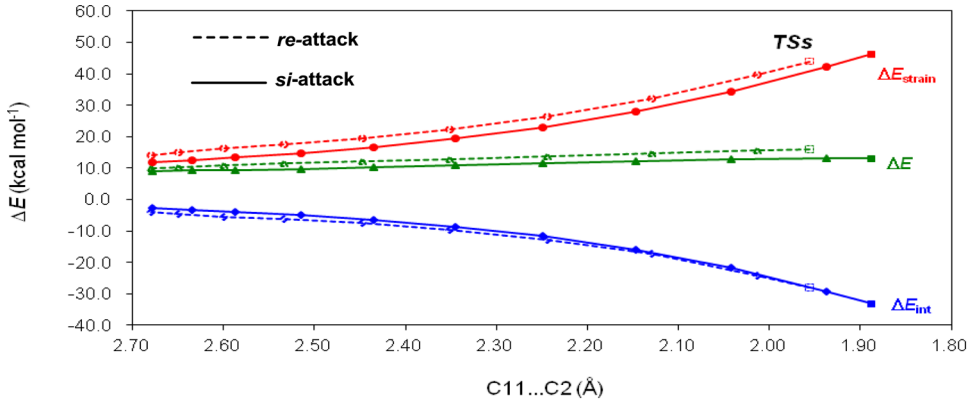

(a)

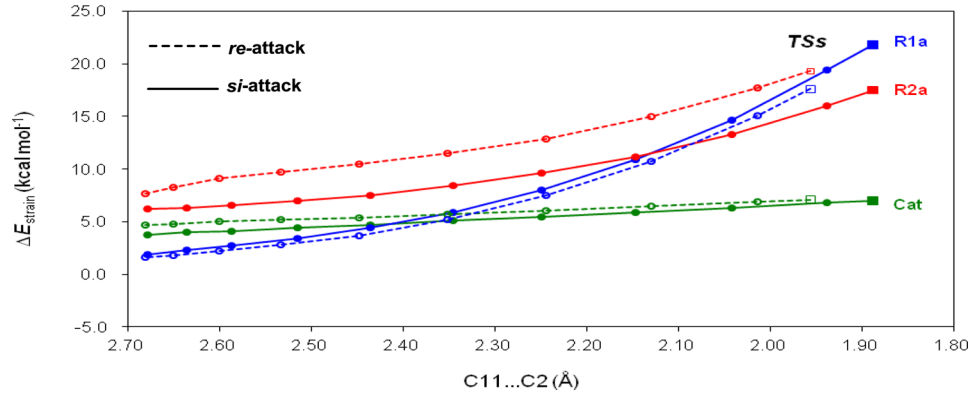

(b)

Figure 6. Activation strain analysis of the carbonyl-ene reaction between *N*-methyl-protected isatin (**R1a**) and 2-methoxypropene (**R2a**) catalyzed by the **L1**−Mg(II) complex catalyst along the reaction coordinate projected onto the C11···C2 distance. (a) Evolution of ΔE, ΔE_{int}, and ΔE_{strain} along the reaction coordinate. (b) Evolution of ΔE_{strain} of three energy components along the reaction coordinate.

stronger destabilization in the ΔE_{strain} curve of the catalyst fragment was observed for *re*-face attack, especially in the early stages of the process. This effect came from significant geometrical deformation of the catalyst moiety due to steric repulsion from the neighboring *ortho* substituent of the ligand in the *re*-face attack pathway. The strain energy for both **R1a** and **R2a** fragments increased remarkably as two reactants approached each other. In the transition state region, the ΔE_{strain} of **R1a** became more destabilizing than that of the **R2a** moiety because of increasingly geometrical distortion. Interestingly, the difference in strain energy ($\Delta\Delta E_{strain}$) caused by the **R2a** substrate was larger than those of the catalyst moiety and the **R1a** moiety in two competing processes. As shown in Figure 6b, the destabilizing effect of ΔE_{strain} of **R2a** on the *si*-face attack pathway was clearly weaker than that computed for the *re*-face attack pathway at any given point along the reaction. A good linear correlation between the C10−C11 bond length in **R2a** and the corresponding strain energy in two pathways was observed (R^2 = 0.997), indicating C10−C11 bond elongation in the ene moiety may be mainly responsible for its deformation energy (see Figure S6). The slope of eq 2a (*re*-face attack) was larger than that of eq 2b (*si*-face attack), suggesting the ΔE_{strain} was more sensitive to geometrical variation of **R2a** in the *re*-face attack pathway. Therefore, the selectivity was mainly caused by an unfavorable steric arrangement along the reaction coordinate in the *re*-face attack pathway, which translated into a more destabilizing activation strain of **R2a**. The difference in strain energy in the **R2a** substrate played an important role in enhancing the stereodifference of two pathways.

The *G* parameter obtained by the Solid-G program helps one to understand the character of the chiral environment of the *N*,*N*′-dioxide−Mg(II) complex and gain insight into the enantioselectivity of the reaction.[45] The steric hindrance of the individual chiral ligand could be described as a percentage of the metal coordination sphere shielded by the ligand, G(L). Because significant structural deformation of fragments occurred mainly in the chirality-controlling step (C−C bond formation step), we focused on only this step to analyze the chiral inductive effect of the catalyst. For **L1**−**COM**, the percentage of the metal center coordination sphere shielded by *N*,*N*′-dioxide ligand **L1** was predicted to be 72.18% [G(**L1**)]. The four bulky 2,6-*i*Pr groups increased the sphere shielded overlap area between **L1** and **R1a** in **L1**−**COM** [G_γ(**L1**) = 2.32%], indicating unfavorable ligand−**R1a** interactions within complex **L1**−**COM**, especially for the *re*-face attack direction (gray area in Figure 3). For C−C bond formation transition states, the G(**L1**) values were 69.17% for **L1**−**TS1**-***si*** and 67.97% for **L1**−**TS1**-***re***. A slightly larger variance for **L1**−**TS1**-***re*** (4.21%, termed **L1**−**COM**) in the *G* parameter reflected a larger distortion of the ligand moiety (especially for the amide moiety) in the formation of the transition state. These results

DOI: 10.1021/acs.joc.6b01071
J. Org. Chem. 2016, 81, 6444−6456

Table 3. Relative Gibbs Free Energies (ΔG, kilocalories per mole) and Differences (ΔΔG, kilocalories per mole) of Two Competing Transition States in the Chirality-Controlling Step[a]

amino acid skeleton	ligand	substituent	TS	ΔG	ΔΔG[b]	ee %[c]
(*S*)-ramipril	**L1**	2,6-*i*Pr	**L1−TS1-*si***	19.1	2.9	98.2 (>99)[d]
			L1−TS1-*re*	22.0		
	L2	2-*i*Pr	**L2−TS1-*si*-a**	13.8	0.4	37.7
			L2−TS1-*re*-d	14.2		
	L3	H	**L3−TS1-*si***	16.5	0.5	44.3
			L3−TS1-*re*	17.0		
	L4	cyclohexane	**L4−TS1-*si***	15.1	0.5	37.7
			L4−TS1-*re*	15.6		
L-prolinol	**L5**	2 -*i*Pr	**L5−TS1-*si***	15.0	0.2	11.9
			L5−TS1-*re*	15.2		
–	**N-L1**	2,6-*i*Pr	**N-L1−TS1-*si***	14.5	3.4	99.3
			N-L1−TS1-*re*	17.9		

[a]The stereoselectivity of the catalytic reaction (ee %) was predicted theoretically by eq 3 of ref 47. [b]The relative Gibbs free energy of the *si*-face attack transition state was set to zero. [c]The ee % was calculated in ref 47. [d]The ee % obtained in the experiment.[27a]

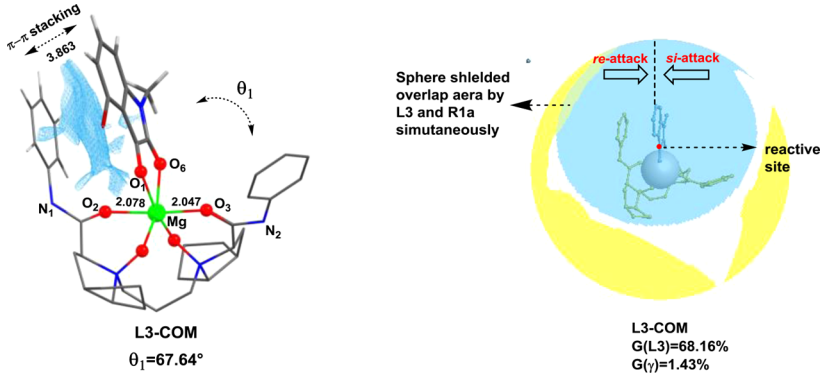

Figure 7. Optimized geometry of **L3−COM** formed by coordinating **R2a** to the **L3**−Mg(II) complex. $\pi-\pi$ stacking was visualized by Multiwfn software (isovalue = 0.8). G(**L3**) was the percentage of the metal center coordination sphere shielded by the *N*,*N*′-dioxide ligand obtained by the Solid-G program. G_γ is the sphere-shielded overlap area of **L3** and **R1a**, simultaneously.

were in agreement with the more destabilizing strain energy of the *N*,*N*′-dioxide−Mg(II) moiety for *re*-face attack (Figure 6, Table S3, and the Supporting Information).

To explore further the origin of the stereocontrolling effect of the chiral catalyst and gain insight into the key structral units of the ligand for asymmetric induction, four more ligands (**L2**−**L5**) were considered at the same theoretical level. The difference in relative Gibbs free energies (ΔΔ*G*) of the two competitive TSs were calculated to evaluate reaction enantioselectivity [ee % value (listed in Table 3)]. For **L2**, one of two *i*Pr groups on each amine moiety in **L1** was removed. Eight possible transition states corresponding to the C−C bond formation step as well as H transfer step were optimized (see Figure S7). Calculations indicated that a pair of competing TSs with the lowest relative energies were **L2−TS1-*si*-a** (*si*-face attack) and **L2−TS1-*re*-d** (*re*-face attack). In these two TSs, the bulky *i*Pr groups at the *ortho* position of aniline in ligands were placed preferentially away from the adjacent aliphatic ring of the chiral backbone and methyl group of the incoming 2-methoxypropene (**R2a**) to prevent steric repulsion. For **L2−TS1-*re*-a**, lacking a block from the second *ortho* *i*Pr substituent, the 2-isopropylphenyl group became more flexible and could rotate along the C−C bond to make more space for the attack of **R2a**. As a result, the relative energy of **L2−TS1-*re*-d** was only 0.4 kcal mol^{-1} higher than that of **L2−TS1-*si*-a**. The difference in their relative energies (ΔΔ*G*) and predicted selectivity of products were significantly decreased compared to those of **L1** with four *i*Pr groups (from 2.9 to 0.4 kcal mol^{-1} and from 98.2 to 37.7%). It seemed that the two bulky isopropoxy groups at the *ortho* position of each amide unit were necessary to form a suitable chiral pocket for high enantioselectivity. When all 2,6-*i*Pr groups were removed (**L3**), the ligand's conformational flexibility made phenyl groups tend to be placed in the same plane to the carbonyl of amines. Accordingly, the chiral cavity of the catalyst became larger, with the angle of two phenyl groups in anilines of 62.38°. Furthermore, angle θ_1 reached 67.64°. The *G* parameter of **L3** was lower than G(**L1**) by 4.02%, indicating that the chiral *N*,*N*′-dioxide shielded the central metal to a lower extent in the **L3−COM** complex. As shown in Figure 7, the distance between the phenyl group of the amide and **R1a** was 3.863 Å. A significant $\pi-\pi$ stacking effect between the substrate and ligand was observed. Lacking repulsion between the *ortho* position substituent of amide moieties, **R2a** could easily approach the coordinated **R1a** from either the *si*-face or the *re*-face (Figure S8). The favorable $\pi-\pi$ stacking effect also increased the stability of the two competing TSs, and the activation barriers for the C−C bond formation step were reduced by 2.6 and 5.0 kcal mol^{-1} compared to that of **L1**−Mg(II)-catalyzed reaction (see Table 3). However, ASM analysis indicated that $\Delta E^{\ddagger}_{int}$ (−28.7 kcal mol^{-1} vs −27.2 kcal mol^{-1}) and $\Delta E^{\ddagger}_{strain}$ (37.4 kcal mol^{-1} vs 36.6 kcal mol^{-1}) (Table S3) were comparable in the formation of **L3−TS1-*si*** and **L3−TS1-*re***, leading to the low ΔΔ*G* (0.5 kcal mol^{-1}) as well as stereoselectivity (44.3%). The

DOI: 10.1021/acs.joc.6b01071
J. Org. Chem. 2016, 81, 6444−6456

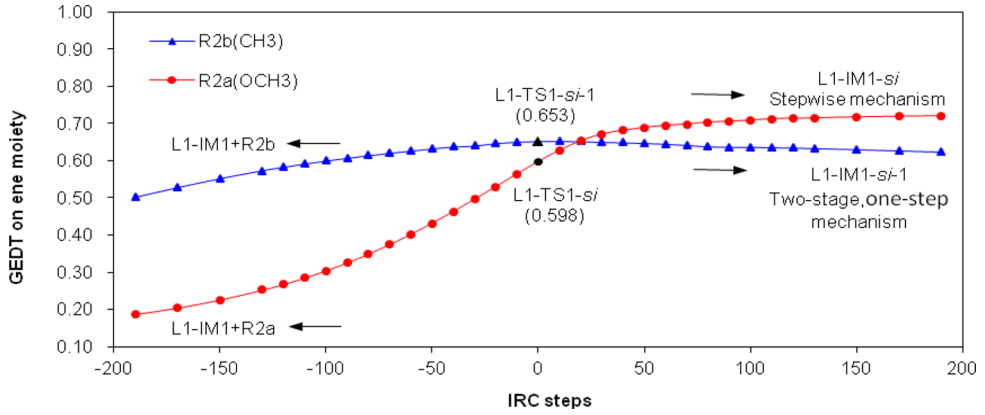

Figure 8. Evolution of GEDT in the formation of the C−C bond in the carbonyl-ene reaction of *N*-methyl-protected isatin (**R1a**) with 2-methoxypropene (**R2a**) and 2-methylpropene (**R2b**) catalyzed by the **L1**−Mg(II) complex catalyst.

effect of the position of the substituent on the phenyl group of amide on the preferential approach direction of the nucleophile was also reported in our previous calculations.[46] For **L4**−**COM** containing aliphatic cyclohexane, the *G* parameter was predicted to be 67.62%. Two six-membered rings moved far from **R1a**, and the angles between **R1a** and the two aliphatic cyclohexanes were ∼55.8° (θ_1) and ∼47.5° (θ_2). Both the O2···O3 distance (4.124 Å) and the O2−Mg−O3 angle (175.6°) were larger than those of **L1**−**COM**, indicating a larger and more open chiral pocket around the Mg(II) ion center. The calculated $\Delta\Delta G$ for the chirality-controlling step was as low as 0.5 kcal mol^{-1}, indicating an inferior chiral induction effect for the **L4**−Mg(II) complex. The effect of steric hindrance from the chiral amide acid backbone was further studied. As expected, the selectivity was decreased when one of the five-membered aliphatic rings in alkyl amine oxide subunits was removed in **L5** (11.9%) because of weakening of the nonbonding interaction. These results suggested that the steric hindrance from both the chiral backbone and the *ortho* position substituent of aniline in the ligand contributed to the chiral inductive effect of the catalyst. For comparison, Mg(OTf)$_2$-catalyzed carbonyl-ene reaction was also studied in the absence of a chiral ligand. Although the reaction could occur easily with lower energy barriers (13.0 and 12.1 kcal mol^{-1} for *si*-face attack and 12.4 and 12.0 kcal mol^{-1} for *re*-face attack), the selectivity was very low because of the lack of a chiral module. The $\Delta\Delta G$ was predicted to be 0.6 kcal mol^{-1} for the C−C bond formation step and 0.1 kcal mol^{-1} for the H transfer step.

Therefore, the combination of chiral *N*,*N*′-dioxide **L1** with Mg(II) ion could form a good chiral Lewis acid catalyst for asymmetric carbonyl-ene reaction. The aromatic rings of amide moieties assisted by the ramipril chiral backbone could form a "pocketlike" chiral environment (chiral pocket) around the central metal ion to achieve a stereoinductive effect. Introducing bulky isopropoxy substituents into *ortho* positions of aniline on amide moieties could alter the space arrangement of aniline and yield a suitable chiral environment, consequently generating a good level of enantiodifferentiation for favorable *si*-face nucleophilic attack. The repulsion between the *i*Pr substituent of the amide in the *N*,*N*′-dioxide ligand and the methyl group of **R2a** as well as the chiral backbone played a key role in achieving the high enanotioselectivity of the asymmetric carbonyl-ene reaction.

Effect of the Substituent of Ene on the Mechanism. To understand the effect of the substituent of the ene reactant on the mechanism, the carbonyl-ene reaction between **R1a** and 2-methylpropene (**R2b**) catalyzed by the **L1**−Mg(II) catalyst was further investigated at the same theoretical level. In contrast to **R2a**, the ene reaction for **R2b** occurred through a one-step mechanism (not stepwise one) when the -OCH$_3$ in **R2a** was replaced with a -CH$_3$ group. The mechanisms of the two competing pathways (*si*-face and *re*-face attack on the prochiral center of **R2a**) were very similar; thus, the one involving favorable *si*-attack is discussed herein. Calculations predicted the energy barriers to be 25.9 kcal mol^{-1} via **L1**−**TS1**-***si*-1**, which was lower than that of the background reaction (34.2 kcal mol^{-1}). These results indicated that the carbonyl-ene reaction between **R1a** and **R2b** could also be facilitated by the Lewis acid Mg(II)−complex catalyst.[1,18,25]

Polar ene reactions are usually related to significant global electron density transfer (GEDT)[48] between two moieties at the corresponding TS. Then, the evolution of the electronic population along the reaction paths was analyzed. As shown in Figure 8, the global electron density transfer occurred from the **R2a** or **R2b** moiety to the coordinated **R1a** moiety via **L1**−**TS1**-***si*** or **L1**−**TS1**-***si*-1**, accompanied by the formation of a C−C bond. This nucleophilic attack developed an excess of electron density within the elecrophilic framework. As a result, the negative charge accumulated on the O1 atom increased, indicating its enhanced nucleophilicity. Although the net global electron density transfer of 0.653 *e* in **L1**−**TS1**-***si*-1** was larger than that in **L1**−**TS1**-***si*** (0.598 *e*), the magnitude of charge variation for the **R2b** moiety was narrower than that of the **R2a** moiety. These results were attributed to the retro-donation process of negative charge from the O1 atom to the H8 atom accompanied by O−H bond formation in **L1**−**TS1**-***si*-1**. For **L1**−**TS1**-***si***, there was interaction between the -OCH$_3$ group and the C═C bond of the **R2a** moiety, with a large stabilization energy between a lone pair on the O atom and the antibonding orbital of C10−C11 [LpO → BD*(π)C10−C11]. Furthermore, this interaction was further strengthened during the formation of the C−C bond, which could be verified by the increasing trend of the Wiberg bond index between the -O(CH$_3$) group and the C10 atom (Figure S9). Consequently, the lack of electron density at the C9 atom in the **R2a** moiety could be compensated by electro-releasing the -OCH$_3$ group, with a slight increase in the negative charge that accumulated on it (see Figure S10). Therefore, the zwitterionic intermediates **L1**−**IM1**-***si*** could be stabilized well, assisted by the -OCH$_3$ group of the **R2a** moiety. The effect of the substituent

DOI: 10.1021/acs.joc.6b01071
J. Org. Chem. 2016, 81, 6444−6456

of the reactants on the mechanism by its participation in global electron density transfer was also observed in our previous work.[43]

Design of a New Ligand. Inspired by the structural character of chiral *N,N′*-dioxide compounds and the chiral phosphine ligand in enantioselective catalysis,[14a,15,24,49,50] we designed one new ligand (**N-L1**) by replacing *N*-oxide units with P donors. The optimized geometries of metal complexes **N-L1−COM** containing the **R1a** substrate are shown in Figure 9.

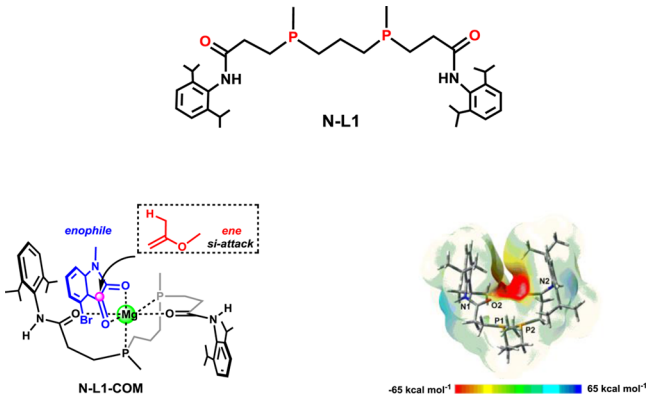

Figure 9. New ligand (**N-L1**) and hexacoordinate-Mg(II) complex, **N-L1−COM**, formed by coordinating **N-L1** and **R1a** to the Mg(II) metal center. The electrostatic potential of the ligand in **N-L1−COM** is shown.

Each symmetric moiety in **N-L1** was also connected by an alkyl linkage containing three CH_2 units, and the ligand's structure featured a metal-centered spirocycle in which the two (C═O)−metal−P six-membered rings were in perpendicular planes. The average donor−metal (P−Mg) distance was ∼2.674 Å, which was longer than the (N)O−Mg bond (2.013 Å) in chiral *N,N′*-dioxide−Mg(II) complex **L1−COM**. Electrostatic potential analysis indicated that the negative charge density was localized on a four-coordinated atom. NBO analysis indicated that there were interactions between the P atom and the Mg atom with stabilization energies of 81 kcal mol^{-1} (LpP1 → Lp*Mg) and 72.4 kcal mol^{-1} (LpP2 → Lp*Mg). Interestingly, the distances between the coordinated O atom of carbonyl groups and Mg(II) were shorter than those of chiral *N,N′*-dioxide−Mg(II) complexes, indicating a stronger coordination interaction of carbonyl groups in **N-L1−COM**. As a result, the "chiral pocket" formed by two amide units and the chiral skeleton was contracted significantly with a decrease in the O2···O3 distance (4.073 Å, vs 4.089 Å in **L1−COM**) and O2−Mg−O3 ligand bite angle (170.6°, vs 172.2° in **L1−COM**). A smaller cavity around the central metal was formed compared to that in the **L1**−Mg(II) complex (**L1−COM**). As expected, the *G* parameters of **N-L1−COM** were decreased because it lacked a bulky aliphatic ring in the backbone and the P donor was slightly far from the metal center (2.674 Å). However, the sphere-shielded overlap area between **N-L1** and **R1a** in **N-L1−COM** increased [G_γ(**N-L1**) = 3.85% vs G_γ(**L1**) = 2.32% (see Figure 10)], indicating more significant blocking for the *re*-face of coordinated **R1a**. By using a weak electron-donor unit (P donor), the Lewis acidity of the metal center in the Mg(II) complex was enhanced. Accordingly, **R1a** was weakened significantly, with the C2−O1 bond (1.231 Å) being longer than that of **L1−COM** (1.228 Å). For comparison, the reaction mechanism of the asymmetric carbonyl-ene reaction between **R1a** and **R2a** catalyzed by the new **N-L1**−Mg(II) complex catalyst was investigated at the same theoretical level. Although the reaction occurred along a similar stepwise pathway, the energy barriers for C−C bond formation (14.5 kcal mol^{-1} for *si*-face attack and 17.9 kcal mol^{-1} for *re*-face attack) as well as H transfer step (14.8 and 17.8 kcal mol^{-1}) were decreased (see Figure 11). The stronger catalytic activation may be attributed to its enhanced electrophilicity (ω = 5.69 eV). Interestingly, the relative energy difference for two competitive transition states and the predicted ee value were increased in the chirality-controlling step compared with those of **L1**−Mg(II) (3.4 kcal mol^{-1} and 99.3% ee). These results indicated that better stereoselectivity could be obtained for the carbonyl-ene reaction of alkyl enol ethers catalyzed by **N-L1**−Mg(II) catalysts. The smaller "chiral pocket" made the steric repulsion from 2,6-*i*Pr groups become more significant in **N-L1−TS1-*re***. One 2,6-*i*Pr group in the amide in **N-L1−TS1-*re*** was pushed away from the **R2a** moiety (the C14−C13−N1−C12 dihedral angle was 80.3°), leading to more significant structural deformation of ligand **N-L1**. As a result, the relative energy of **N-L1−TS1-*re*** was higher than that of **N-L1−TS1-*si*** by 3.4 kcal mol^{-1} (see Table 3). Therefore, the coordination environment and Lewis acidity of the chiral ligand−Mg(II) catalyst could be fine-tuned by introducing P-donor units into the ligand. **N-L1** could be a better ligand for

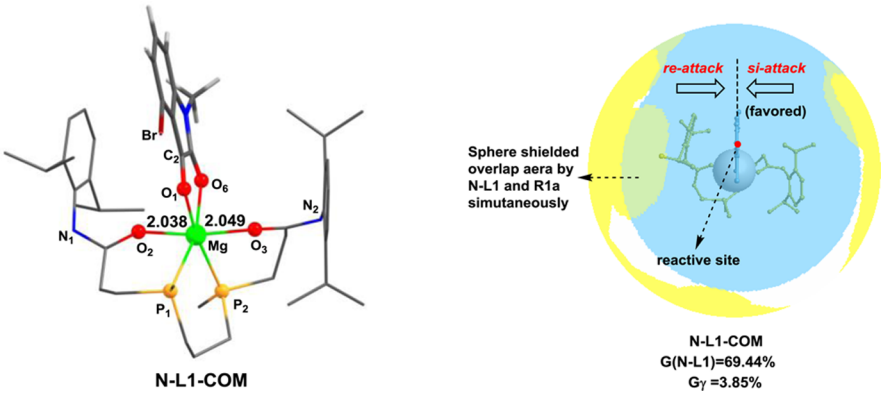

Figure 10. Optimized geometries of the new ligand (**N-L1**) and *G*(**L1**) as the percentage of metal center coordination sphere shieldrf by the *N,N′*-dioxide ligand obtained by the Solid-G program. G_γ is the sphere-shielded overlap area of **N-L1** and **R1a**, simultaneously.

DOI: 10.1021/acs.joc.6b01071
J. Org. Chem. 2016, 81, 6444−6456

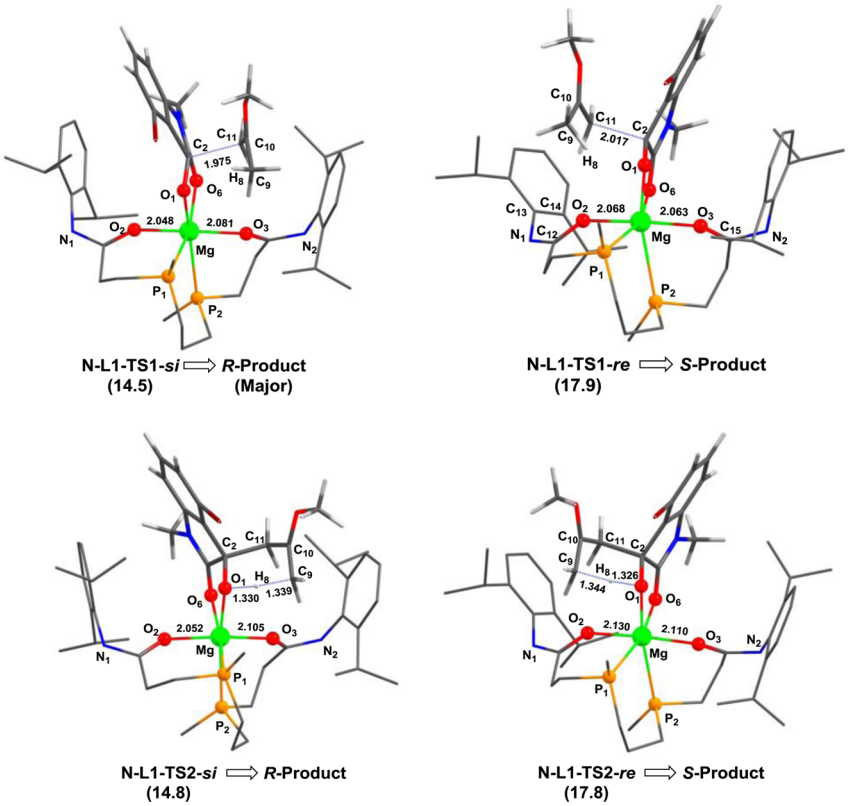

Figure 11. Optimized geometries of the transition states and relative Gibbs free energies (kilocalories per mole) for C−C bond formation and hydrogen transfer steps in the carbonyl-ene reaction between *N*-methyl-protected isatin (**R1a**) and 2-methoxypropene (**R2a**) catalyzed by the **N-L1**−Mg(II) complex.

forming a metal complex catalyst for asymmetric carbonyl-ene reaction.

CONCLUSION

Theoretical investigation of the asymmetric addition of 2-methyl enol ethers to *N*-methyl-protected isatin catalyzed by the *N*,*N*′-dioxide−$Mg(OTf)_2$ complex revealed the following results.

(1) The background reaction occurred along a one-step, two-stage mechanism with a high activation barrier of 30.4 kcal mol^{-1}. Good linear correlations between the global nucleophilicity index (N) and the activation energy barrier ($\Delta G^{\ddagger}$) were found (R^2 = 0.97).

(2) The chiral *N*,*N*′-dioxide−Mg(II) complex catalyst could enhance the electrophilicity of the isatin substrate by coordinating O atoms of the dicarbonyl compound to the Mg(II) metal center in a bidentate model to form hexacoordinate Mg(II) reactive species, accelerating the ene reaction through a more polar process with lower activation barriers. The *ortho*-substituted aniline of the amide combined with the aliphatic ring of the ligand backbone in chiral *N*,*N*′-dioxide constructed an favorable "pocketlike" chiral environment (chiral pocket) around the Mg(II) center for the asymmetric carbonyl-ene reaction. The repulsion between the isopropyl substituent of amide in *N*,*N*′-dioxide ligand and the methyl group of **R2a** as well as the chiral backbone played a key role in achieving the high enanotioselectivity of products by blocking the reactive site from unfavorable *re*-attack. The difference in strain energy in the **R2a** substrate enhanced enantiodifferentiation of two pathways, ensuring the desired *R* product.

(3) This work suggests a new chiral ligand (**N-L1**) via substitution of *N*-oxide units in *N*,*N*′-dioxide ligand (**L1**) with a P-donor moiety. The improved Lewis acidity of the Mg(II) complex catalyst and the chiral environment could be realized by adjusting the coordination interaction between the carbonyl groups and the P donor of the ligand to metal center.

ASSOCIATED CONTENT

Supporting Information

The Supporting Information is available free of charge on the ACS Publications website at DOI: 10.1021/acs.joc.6b01071.

Cartesian coordinates of all stationary points and energies; global and local reactivity indices of reacting sites as well as electrophilicity−nucleophilicity indices E_1 and E_2; results of the activation strain model (ASM) in noncatalytic and catalytic carbonyl-ene reactions; evolution of Wiberg bond index C10−O(CH_3) and NPA charge on the C9 atom during the formation of the C−C bond for the carbonyl-ene reaction catalyzed by the **L1**−Mg(II) complex; and correlation between ΔE_{12} and $\Delta G^{\ddagger}$, log k, and $\Delta E^{\ddagger}_{int}$ for the carbonyl-ene reaction in the background reaction (PDF)

AUTHOR INFORMATION

Corresponding Author

*E-mail: suzhishan@scu.edu.cn.

Notes

The authors declare no competing financial interest.

DOI: 10.1021/acs.joc.6b01071
J. Org. Chem. 2016, 81, 6444−6456

■ ACKNOWLEDGMENTS

We thank the National Natural Science Foundation of China (21290182, 21321061, and 21572141) and the Program for New Century Excellent Talents in University of China (NCET-13-0390) for financial support.

■ REFERENCES

(1) (a) Mikami, K.; Shimizu, M. *Chem. Rev.* **1992**, *92*, 1021−1050. (b) Thomas, B. E.; Loncharich, R. J.; Houk, K. N. *J. Org. Chem.* **1992**, *57*, 1354−1362.
(2) Alder, K.; Pascher, F.; Schmitz, A. *Ber. Dtsch. Chem. Ges. B* **1943**, *76*, 27−53.
(3) Hoffmann, H. M. R. *Angew. Chem., Int. Ed.* **1969**, *8*, 556−577.
(4) Snider, B. B. *Acc. Chem. Res.* **1980**, *13*, 426−432.
(5) Dubac, J.; Laporterie, A. *Chem. Rev.* **1987**, *87*, 319−334.
(6) Snider, B. B. *Comprehensive Organic Synthesis* **1991**, *2*, 527−561.
(7) Clarke, M. L.; France, M. B. *Tetrahedron* **2008**, *64*, 9003−9031.
(8) Maruoka, K.; Hoshino, Y.; Shirasaka, T.; Yamamoto, H. *Tetrahedron Lett.* **1988**, *29*, 3967−3970.
(9) (a) Mikami, K.; Terada, M.; Nakai, T. *J. Am. Chem. Soc.* **1989**, *111*, 1940−1941. (b) Mikami, K.; Terada, M.; Nakai, T. *J. Am. Chem. Soc.* **1990**, *112*, 3949−3954. (c) Mikami, K.; Matsukawa, S. *J. Am. Chem. Soc.* **1993**, *115*, 7039−7040. (d) Mikami, K.; Yajima, T.; Takasaki, T.; Matsukawa, S.; Terada, M.; Uchimaru, T.; Maruta, M. *Tetrahedron* **1996**, *52* (1), 85−98.
(10) (a) Evans, D. A.; Burgey, C. S.; Paras, N. A.; Vojkovsky, T.; Tregay, S. W. *J. Am. Chem. Soc.* **1998**, *120*, 5824−5825. (b) Evans, D. A.; Tregay, S. W.; Burgey, C. S.; Paras, N. A.; Vojkovsky, T. *J. Am. Chem. Soc.* **2000**, *122*, 7936−7943.
(11) Evans, D. A.; Wu, J. *J. Am. Chem. Soc.* **2005**, *127*, 8006−8007.
(12) (a) Zhao, J. F.; Tjan, T. B. W.; Tan, B. H.; Loh, T. P. *Org. Lett.* **2009**, *11* (24), 5714−5716. (b) Zhao, J. F.; Tsui, H. Y.; Wu, P. J.; Lu, J.; Loh, T. P. *J. Am. Chem. Soc.* **2008**, *130*, 16492−16493. (c) Zhao, J. F.; Tan, B. H.; Zhu, M. K.; Tjan, T. B. W.; Loh, T. P. *Adv. Synth. Catal.* **2010**, *352*, 2085−2088. (d) Lu, J.; Hong, M. L.; Ji, S. J.; Loh, T. P. *Chem. Commun.* **2005**, 1010−1012.
(13) (a) Kezuka, S.; Ikeno, T.; Yamada, T. *Org. Lett.* **2001**, *3*, 1937−1939. (b) Kezuka, S.; Kogami, Y.; Ikeno, T.; Yamada, T. *Bull. Chem. Soc. Jpn.* **2003**, *76*, 49−58. (c) Hutson, G. E.; Dave, A. H.; Rawal, V. H. *Org. Lett.* **2007**, *9*, 3869−3872.
(14) (a) Mikami, K.; Kawakami, Y.; Akiyama, K.; Aikawa, K. *J. Am. Chem. Soc.* **2007**, *129*, 12950−12951. (b) Hao, J.; Hatano, M.; Mikami, K. *Org. Lett.* **2000**, *2*, 4059−4062. (c) Aikawa, K.; Kainuma, S.; Hatano, M.; Mikami, K. *Tetrahedron Lett.* **2004**, *45*, 183−185. (d) Hatano, M.; Mikami, K. *J. Am. Chem. Soc.* **2003**, *125*, 4704−4705. (e) Doherty, S.; Knight, J. G.; Smyth, C. H.; Harrington, R. W.; Clegg, W. *J. Org. Chem.* **2006**, *71*, 9751−9764.
(15) Koh, J. H.; Larsen, A. O.; Gagné, M. R. *Org. Lett.* **2001**, *3*, 1233−1236.
(16) (a) Ruck, R. T.; Jacobsen, E. N. *Angew. Chem., Int. Ed.* **2003**, *42*, 4771−4774. (b) Grachan, M. L.; Tudge, M. T.; Jacobsen, E. N. *Angew. Chem., Int. Ed.* **2008**, *47*, 1469−1472. (c) Ruck, R. T.; Jacobsen, E. N. *J. Am. Chem. Soc.* **2002**, *124*, 2882−2883.
(17) Qian, C. T.; Wang, L. C. *Tetrahedron: Asymmetry* **2000**, *11*, 2347−2357.
(18) Domingo, L. R.; Aurell, M. J.; Pérez, P. *Org. Biomol. Chem.* **2014**, *12*, 7581−7590.
(19) (a) Leach, A. G.; Houk, K. N. *Org. Biomol. Chem.* **2003**, *1*, 1389−1403. (b) Leach, A. G.; Houk, K. N. *Chem. Commun.* **2002**, 1243−1255.
(20) Sakai, S.; Hikida, T. *J. Phys. Chem. A* **2008**, *112*, 10985−10992.
(21) Candito, D. A.; Dobrovolsky, D.; Lautens, M. *J. Am. Chem. Soc.* **2012**, *134*, 15572−15580.
(22) Pérez, P.; Domingo, L. R. *Eur. J. Org. Chem.* **2015**, *2015*, 2826−2834.
(23) Ruck, R. T.; Jacobsen, E. N. *J. Am. Chem. Soc.* **2002**, *124*, 2882−2883.
(24) Aikawa, K.; Mimura, S.; Numata, Y.; Mikami, K. *Eur. J. Org. Chem.* **2011**, *2011*, 62−65.
(25) Yang, Q. W.; Liu, Y.; Zhang, W. Q. *Org. Biomol. Chem.* **2011**, *9*, 6343−6351.
(26) (a) Fernandez, I.; Bickelhaupt, F. M. *J. Comput. Chem.* **2012**, *33*, 509−516. (b) Jin, R.; Liu, S.; Lan, Y. *RSC Adv.* **2015**, *5*, 61426−61435.
(27) (a) Zheng, K.; Yin, C. K.; Liu, X. H.; Lin, L. L.; Feng, X. M. *Angew. Chem.* **2011**, *123*, 2621−2625. (b) Zheng, K.; Shi, J.; Liu, X. H.; Feng, X. M. *J. Am. Chem. Soc.* **2008**, *130*, 15770−15771. (c) Liu, X. H.; Lin, L. L.; Feng, X. M. *Acc. Chem. Res.* **2011**, *44*, 574−587. (d) Liu, X. H.; Lin, L. L.; Feng, X. M. *Org. Chem. Front.* **2014**, *1*, 298−302. (e) Shen, K.; Liu, X. H.; Lin, L. L.; Feng, X. M. *Chem. Sci.* **2012**, *3*, 327−334.
(28) Frisch, M. J.; Trucks, G. W.; Schlegel, H. B.; Scuseria, G. E.; Robb, M. A.; Cheeseman, J. R.; Scalmani, G.; Barone, V.; Mennucci, B.; Petersson, G. A.; Nakatsuji, H.; Caricato, M.; Li, X.; Hratchian, H. P.; Izmaylov, A. F.; Bloino, J.; Zheng, G.; Sonnenberg, J. L.; Hada, M.; Ehara, M.; Toyota, K.; Fukuda, R.; Hasegawa, J.; Ishida, M.; Nakajima, T.; Honda, Y.; Kitao, O.; Nakai, H.; Vreven, T.; Montgomery, J. A., Jr.; Peralta, J. J. E.; Ogliaro, F.; Bearpark, M.; Heyd, J. J.; Brothers, E.; Kudin, K. N.; Staroverov, V. N.; Keith, T.; Kobayashi, R.; Normand, J.; Raghavachari, K.; Rendell, A.; Burant, J. C.; Iyengar, S. S.; Tomasi, J.; Cossi, M.; Rega, N.; Millam, J. M.; Klene, M.; Knox, J. E.; Cross, J. B.; Bakken, V.; Adamo, C.; Jaramillo, J.; Gomperts, R.; Stratmann, R. E.; Yazyev, O.; Austin, A. J.; Cammi, R.; Pomelli, C.; Ochterski, J. W.; Martin, R. L.; Morokuma, K.; Zakrzewski, V. G.; Voth, G. A.; Salvador, P.; Dannenberg, J. J.; Dapprich, S.; Daniels, A. D.; Farkas, O.; Foresman, J. B.; Ortiz, J. V.; Cioslowski, J.; Fox, D. J. *Gaussian 09*, revision D.01; Gaussian, Inc.: Wallingford, CT, 2013.
(29) Marenich, A. V.; Cramer, C. J.; Truhlar, D. G. *J. Phys. Chem. B* **2009**, *113*, 6378−6396.
(30) (a) Svensson, M.; Humbel, S.; Morokuma, K. *J. Chem. Phys.* **1996**, *105*, 3654−3661. (b) Dapprich, S.; Komáromi, I.; Byun, K. S.; Morokuma, K.; Frisch, M. J. *J. Mol. Struct.: THEOCHEM* **1999**, *461*−*462*, 1−21. (c) Vreven, T.; Morokuma, K. *J. Comput. Chem.* **2000**, *21*, 1419−1432. (d) Chung, L. W.; Sameera, W. M. C.; Ramozzi, R.; Page, A. J.; Hatanaka, M.; Petrova, G. P.; Harris, T. V.; Li, X.; Ke, Z. F.; Liu, F. Y.; Li, H. B.; Ding, L.; Morokuma, K. *Chem. Rev.* **2015**, *115*, 5678−5796.
(31) Rappé, A. K.; Casewit, C. J.; Colwell, K. S.; Goddard, W. A.; Skiff, W. M. *J. Am. Chem. Soc.* **1992**, *114*, 10024−10035.
(32) Becke, A. D. *J. Chem. Phys.* **1993**, *98*, 5648−5652.
(33) Gonzalez, C.; Schlegel, H. B. *J. Chem. Phys.* **1989**, *90*, 2154−2161.
(34) (a) Grimme, S.; Antony, J.; Ehrlich, S.; Krieg, H. *J. Chem. Phys.* **2010**, *132*, 154104−154119. (b) Grimme, S.; Ehrlich, S.; Goerigk, L. *J. Comput. Chem.* **2011**, *32* (7), 1456−1465.
(35) Reed, A. E.; Curtiss, L. A.; Weinhold, F. *Chem. Rev.* **1988**, *88*, 899−926.
(36) (a) Domingo, L. R.; Sáez, J. A. *Org. Biomol. Chem.* **2009**, *7*, 3576−3583. (b) Domingo, L. R.; Chamorro, E.; Pérez, P. *J. Org. Chem.* **2008**, *73*, 4615−4624. (c) Parr, R. G.; Szentpály, L. V.; Liu, S. *J. Am. Chem. Soc.* **1999**, *121*, 1922−1924. (d) Domingo, L. R.; Aurell, M. J.; Pérez, P.; Contreras, R. *Tetrahedron* **2002**, *58*, 4417−4423.
(37) Domingo, L. R.; Pérez, P.; Sáez, J. A. *RSC Adv.* **2013**, *3*, 1486−1494.
(38) (a) Soto-Delgado, J.; Domingo, L. R.; Contreras, R. *Org. Biomol. Chem.* **2010**, *8*, 3678−3683. (b) The reactivity indices E_1 and E_2 are defined by the following expressions: $E_1 = \omega_{DP} + N_D$ and $E_2 = \omega_D + N_{DP}$, where D is the diene moiety and DP the dienophile moiety.[38a] In the work presented here, E_1 is the summary of $\omega_{isatin} + N_{ene}$ and E_2 is the summary of $\omega_{ene} + N_{isatin}$. In this way, if $E_1 > E_2$, the process is expected to exhibit ene moiety to isatin moiety electron flow; if $E_2 > E_1$, the process is expected to exhibit isatin moiety to ene moiety electron flow.
(39) (a) Fernandez, I.; Bickelhaupt, F. M. *Chem. Soc. Rev.* **2014**, *43*, 4953−4967. (b) van Zeist, W.-J.; Bickelhaupt, F. M. *Org. Biomol. Chem.* **2010**, *8*, 3118−3127. (c) Fernandez, I. *Phys. Chem. Chem. Phys.* **2014**, *16*, 7662−7671. (d) Sader, C. A.; Houk, K. N. *arkivoc* **2014**,

DOI: 10.1021/acs.joc.6b01071
J. Org. Chem. 2016, 81, 6444−6456

170−183. (e) Hong, X.; Liang, Y.; Griffith, A. K.; Lambert, T. H.; Houk, K. N. *Chem. Sci.* **2014**, *5*, 471−475. (f) Houk, K. N.; Beno, B. R.; Nendel, M.; Black, K.; Yoo, H. Y.; Wilsey, S.; Lee, J. K. *J. Mol. Struct.: THEOCHEM* **1997**, *389*−*399*, 169−179. (g) Thomas, B. E.; Loncharich, R. J.; Houk, K. N. *J. Org. Chem.* **1992**, *57*, 1354−1362. (h) Ess, D. H.; Houk, K. N. *J. Am. Chem. Soc.* **2007**, *129*, 10646−10647.

(40) Domingo, L. R.; Sáez, J. A.; Zaragoza, R. J.; Arno, M. *J. Org. Chem.* **2008**, *73*, 8791−8799.

(41) Loncharich, R. J.; Houk, K. N. *J. Am. Chem. Soc.* **1987**, *109*, 6947−6952.

(42) Pérez, P.; Domingo, L. R. *Eur. J. Org. Chem.* **2015**, *2015*, 2826−2834.

(43) (a) Su, Z. S.; Qin, S.; Hu, C. W.; Feng, X. M. *Chem. - Eur. J.* **2010**, *16*, 4359−4367. (b) Su, Z. S.; Kim, C. K. *Org. Biomol. Chem.* **2015**, *13*, 6313−6324.

(44) Anslyn, E. V.; Dougherty, D. A. *Modern physical organic chemistry*; University Science Books: Sausalito, CA, 2006.

(45) (a) Guzei, I. A.; Wendt, M. *Dalton Trans.* **2006**, 3991−3999. (b) Marx, F. T. I.; Jordaan, J. H. L.; Lachmann, G.; Vosloo, H. C. M. *J. Comput. Chem.* **2014**, *35*, 1457−1463.

(46) Zhang, Y. L.; Yang, N.; Liu, X. H.; Guo, J.; Zhang, X. Y.; Lin, L. L.; Hu, C. W.; Feng, X. M. *Chem. Commun.* **2015**, *51*, 8432−8435.

(47) Schneebeli, S. T.; Hall, M. L.; Breslow, R.; Friesner, R. *J. Am. Chem. Soc.* **2009**, *131*, 3965−3973.

(48) Domingo, L. R. *RSC Adv.* **2014**, *4*, 32415−32428.

(49) (a) Kozuch, S.; Amatore, C.; Jutand, A.; Shaik, S. *Organometallics* **2005**, *24*, 2319−2330. (b) Kozuch, S.; Shaik, S. *J. Mol. Catal. A: Chem.* **2010**, *324*, 120−126.

(50) Lu, Q. Q.; Yu, H. Z.; Fu, Y. *J. Am. Chem. Soc.* **2014**, *136*, 8252−8260.

DOI: 10.1021/acs.joc.6b01071
J. Org. Chem. 2016, 81, 6444−6456